Reorganization Induced by Silver Salt Reduction Inside a Mesostructured Block Copolymer Silica Film

ARTICLE *in* THE JOURNAL OF PHYSICAL CHEMISTRY C · DECEMBER 2011

Impact Factor: 4.77 · DOI: 10.1021/jp207207x

5 AUTHORS, INCLUDING:

Bois Laurence
Claude Bernard University Lyon 1
90 PUBLICATIONS **1,173** CITATIONS
SEE PROFILE

Arnaud Brioude
Claude Bernard University Lyon 1
108 PUBLICATIONS **1,962** CITATIONS
SEE PROFILE

THE JOURNAL OF PHYSICAL CHEMISTRY C

ARTICLE

pubs.acs.org/JPCC

Reorganization Induced by Silver Salt Reduction Inside a Mesostructured Block Copolymer Silica Film

Fernand Chassagneux,*[,†] Jean-Paul Simon,[§] Laurence Bois,[†] Cedric Desroches,[†] and Arnaud Brioude[†]

[†]Laboratoire des Multimatériaux et Interfaces, UMR CNRS 5615, Bât. Berthollet, Université Claude Bernard - Lyon 1, 43 Bd 11 novembre 1918, 69622 Villeurbanne, France

[§]SIMAP, INP, Grenoble-CNRS-UJF (UMR 5266), BP75, 38402 St Martin d'Hères, France

Supporting Information

ABSTRACT: Block copolymer self-assembly can be used to get a noble metallic nanoparticle array. The silver nanoparticle array formation inside a mesostructured silica film with the triblock copolymer $(PEO)_{106}(PPO)_{70}(PEO)_{106}$ (F127) has been studied using Grazing Incidence Small-Angle X-ray Scattering (GISAXS), TEM, and X-ray diffraction analyses. Mesostructure organization essentially occurs during the sodium borohydride reduction process used to form silver nanoparticles. The well-known orthorhombic order, *Fmmm* space group, appears with $(020)_{orthorhombic}$ plan parallel to the substrate. Such reorganization is explained by the silver ion diffusion occurring along preferential directions toward the film surface. These metallic nanostructures could be potentially used in surface-enhanced Raman scattering, catalysis, or optical devices.

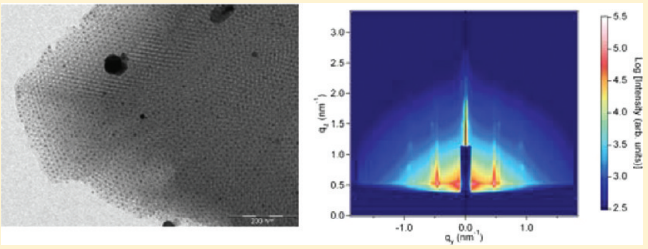

1. INTRODUCTION

Metallic nanoparticles support localized surface-plasmon resonance (LSPR).[1] LSPR is used in various applications, such as biosensing,[2,3] enhancement of Raman scattering, optical data storage, or nonlinear optics.[4,5] Mesostructured inorganic materials such as mesoporous silica films, formed through surfactant self-assembly, can be involved in a templating metallic nanoparticle array.[6−12] Sodium borohydride is often used to synthesize silver nanoparticles in solution[13−16] or to get silver nanoparticle dispersion inside mesoporous materials.[17,18] We have previously used it to elaborate silver nanoparticle assemblies inside hybrid block copolymer oxide films[19−22] prepared by an evaporation-induced self-assembly process (EISA).[23−25] The silver precursor is introduced either directly during synthesis of hybrid block copolymer silica film or after block copolymer elimination using film impregnation in a silver salt solution. Sodium borohydride action on this mesostructured layer with block copolymer F127, $(PEO)_{106}(PPO)_{70}(PEO)_{106}$, is characterized by the formation of metallic nanoparticles concentrated on the top layer along a 10 nm thickness. This metallic repartition has been evidenced by TEM and RBS experiments,[21,22] and films have also been characterized by their surface plasmon resonance (SPR).

Silver nitrate reduction kinetics by $NaBH_4$ in water has been investigated corresponding to a rapid reaction at room temperature.[26,27] Yet, several steps of metallic nanoparticle formation or growth remain misunderstood, influenced in a complex way by ionic strength, capping agent, or surfactant.[27−31] This is naturally true when silver salt reduction occurs inside a thin mesostructured oxide layer.

By using block copolymer F127, a body-centered cubic type arrangement of spherical micelles is usually obtained.[32−34] Such an arrangement is preserved inside a mesoporous layer resulting from block copolymer elimination and has been largely studied.[32−35]

This work explores X-ray diffraction, TEM, and GISAXS (grazing incident small-angle X-ray scattering) data. In this study, we focus our attention on the textural evolution occurring in these hybrid silica-block copolymer layers, first by introducing silver salt during layer synthesis and then by treating the layer either by thermal treatment or in $NaBH_4$ solution.[22]

2. EXPERIMENTAL SECTION

2.1. Synthesis. Simple F127-silica films (F0) synthesis, without silver salt, was described in refs 19 and 35. Silver salt containing films were obtained by modification of F0 film synthesis by inserting silver salt (10% silver to silicon content) during the sol synthesis.[22] Both films were thermally treated at 200 °C (5 °C/min, for 2 h), inducing silver salt reduction in the case of F1, and noted F*x*T. Otherwise, films were immersed in a sodium borohydride solution (0.05 M) during 30 s and noted

Received: July 28, 2011
Revised: October 31, 2011

   dx.doi.org/10.1021/jp207207x | J. Phys. Chem. C XXXX, XXX, 000–000

F*x*N. Silver salt contained in the F1 sample is then strongly reduced with sodium borohydride. The sample description is reported in Table 1 .

2.2. Characterization. The TEM images were taken with a TOPCON EM002B transmission electron microscope operating at 200 keV. Samples for the transmission electron microscopy (TEM) characterization were prepared by scrapping the film. The fragments were then deposed directly on a copper grid coated with holey carbon film. GISAXS experiments were performed at the d2am beamline (11.85 keV) at ESRF (Grenoble). The detector was located at 1092 mm behind the sample, and the exposure time was 10 s. Small-angle X-ray diffraction (XRD) patterns were recorded on a Philips Xpert Pro diffractometer equipped with a monochromator, using Cu Kα radiation.

Table 1. Sample Descriptions

silver content	0%	10%
preparation method		
F127-silica	F0	F1
" " after $NaBH_4$ reduction	F0N	F1N
" " after thermal treatment	F0T	F1T

3. RESULTS AND DISCUSSION

3. 1. Effect of the Presence of Silver Salt on the Textural Properties of Hybrid Block Copolymer Silica Films. *3.1.a. Hybrid Block Copolymer Silica Films.* Hybrid block copolymer—silica films F0 and F1 small-angle XRD patterns are shown in Figure 1a. A shoulder before $2\theta = 1°$ is observed in F0 pattern, while a well-defined peak is noted in F1 pattern. This peak has been generally attributed to {011} reflection of Im-3m structure. More rigorously, it has been indexed as (020) reflection of an orthorhombic *Fmmm* structure, resulting from more or less pronounced layer contraction in the direction perpendicular to the substrate.[36] Interreticular distance $d(011)_{cubic}$ in the case of F0 is calculated at 9.3 nm. This value is to compare with GiSAXS results in Figure 1b. Indeed, from the most intensive ring, the value at 9.6 nm can be measured at $q_y = 0$ in the GISAXS pattern. The ring is due to diffraction of $\{011\}_{cubic}$ plans which are in zone with different crystallographic directions and particularly with the cube edge ⟨100⟩ lying on the film surface.

XRD and GISAXS patterns of silver containing film, F1 sample, in Figures 1a and 1c are qualitatively comparable to patterns previously shown (Figures 1a and 1b). Silver content corresponds to the atomic ratio of silver/silicon of 0.1.

The interreticular distance of 9.2 nm is calculated from the peak ($2\theta = 0.93°$) due to {011} reflection in Im-3m structure (Figure 1a).

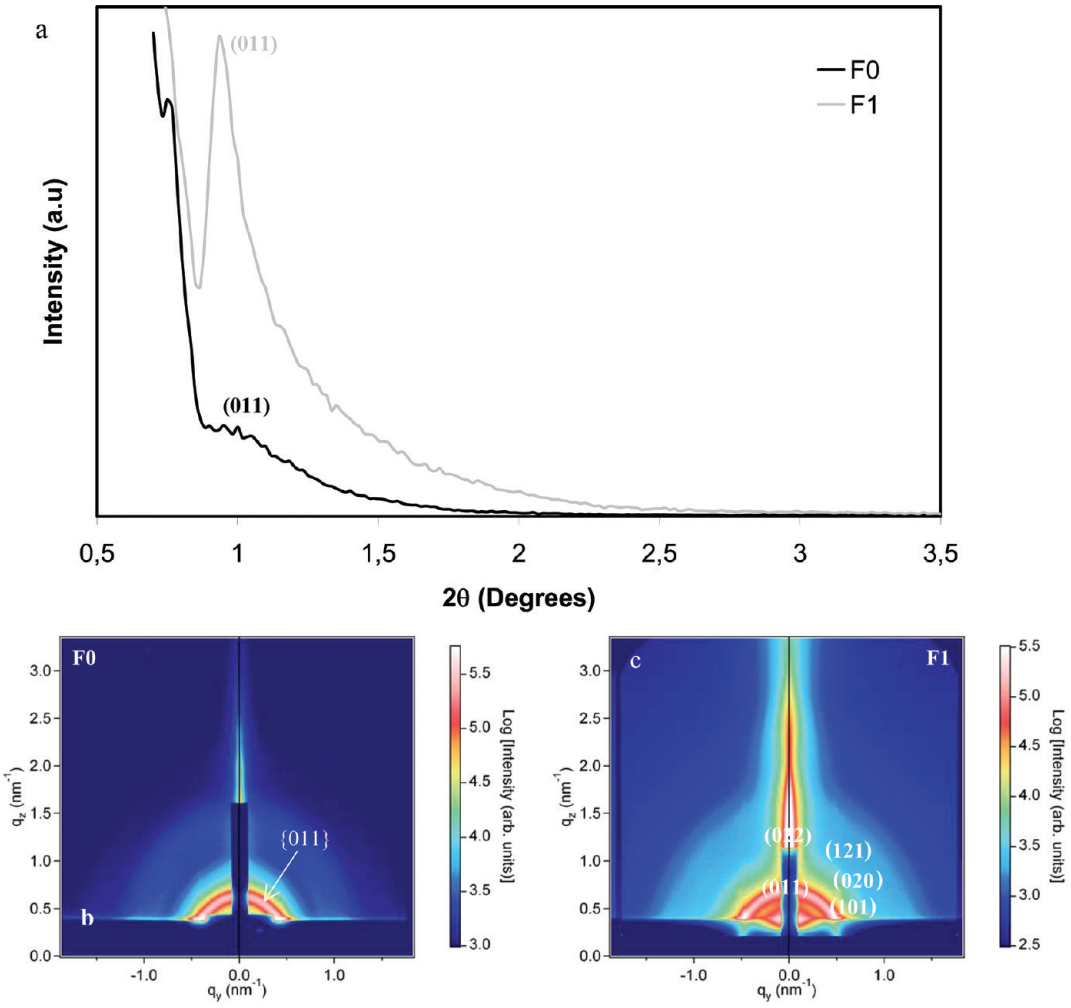

Figure 1. (a) Small-angle XRD patterns of F0 and F1 samples. (b) GISAXS pattern of the F0 sample. (c) GISAXS pattern of the F1 sample cubic indexation.

dx.doi.org/10.1021/jp207207x |*J. Phys. Chem. C* XXXX, XXX, 000–000

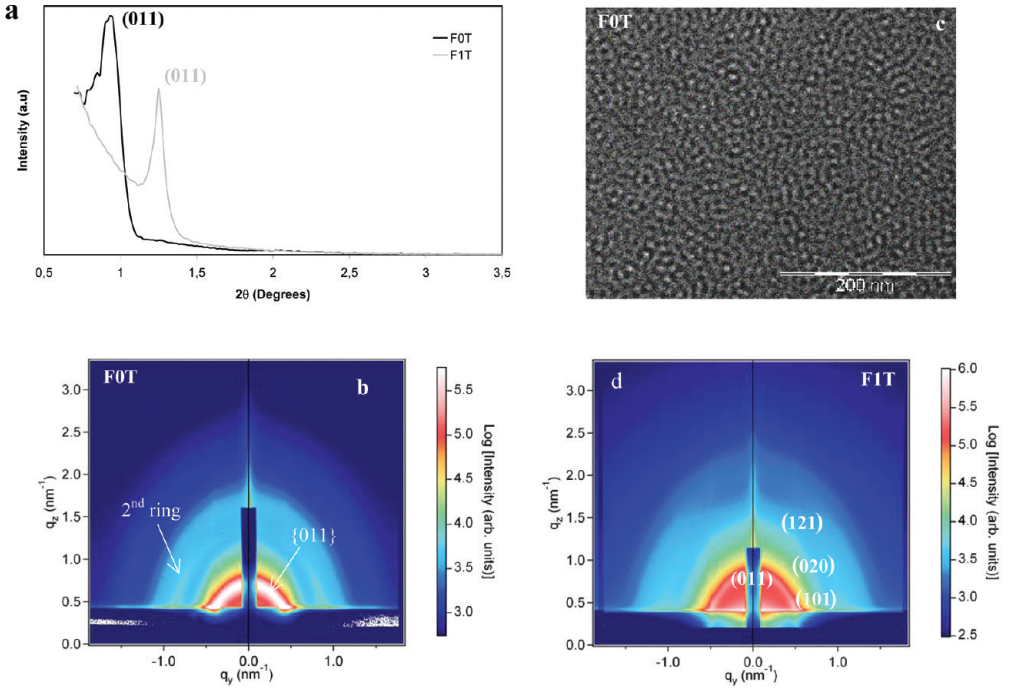

Figure 2. (a) Small-angle XRD patterns of F0T and F1T samples. (b) GISAXS pattern of the F0T sample. (c) TEM top view of the F0T sample. (d) GISAXS pattern of the F1T sample (diffraction spots indexed in Im-3m).

Silver salt addition does not modify the pattern aspect of the GISAXS pattern (Figure 1c), but increasing contrast reveals a slight tendency to layer preferential orientation parallel to the (011) plan in Im-3m structure. $d_{(011)\text{cubic}}$ is measured at 9.2 nm. GISAXS spots are indexed in cubic Im-3m structure.

For a higher silver ratio (Ag/Si > 20%), layers are no more organized (no diffraction peak). This can be explained by silver salt selective accumulation into hydrophilic and external micelle parts, totally modifying electrostatic interactions.

3.1.b. Hybrid Block Copolymer Silica Films after Thermal Treatment. The F0T small angle XRD pattern is shown in Figure 2a. This sample is obtained after a thermal treatment at 200 °C inducing block copolymer elimination. A well-defined peak is noted at $2\theta = 0.93°$ in F0T, attributed to the $\{011\}$ reflection of Im-3m. A few intensive peaks noted at $2\theta = 1.9°$ are due to $(022)_{\text{cubic}}$. Interreticular distance $d(011)_{\text{cubic}}$ is calculated at 9.3 nm. This value is to compare with GiSAXS results in Figure 2b. Indeed, from the most intensive ring, the value at 9.2 nm can be measured at $q_y = 0$ in the GISAXS pattern. Once more, the ring is due to diffraction of $\{011\}_{\text{cubic}}$ plans. Furthermore, a second ring is noted in Figure 2b, due to a higher contrast after block copolymer elimination.[37] There is no layer preferential orientation from pattern 2b, but ring elliptic deformation is noted resulting from layer contraction perpendicular to the substrate. Preferential orientation absence is also observed from the top view TEM showing a vermicular mesostructure (Figure 2c).

After thermal treatment at 200 °C of a silver-containing film, XRD and GISAXS patterns of the F1T sample, in Figures 2a and 2d, are qualitatively comparable to patterns previously shown. Interreticular distance of 7.0 nm ($2\theta = 1.25°$) is calculated from the peak due to $\{011\}_{\text{cubic}}$ (Figure 2a). This diffraction peak is related to much shorter distance compared to the F1 sample before thermal treatment.

The ring noted in Figure 2d (sample F1T) is thinner than the ring observed in F0T; it is also due to a shorter interreticular distance along q_z. The same remark can be done concerning XRD and GISAXS patterns of samples F1T and F1. Indeed, $d_{(011)\text{cubic}}$ in F1T is measured at 7.6 nm. Such a difference is due to the higher layer contraction perpendicular to the substrate than previously noted. On the contrary, $d_{(101)\text{cubic}}$ is almost unchanged as there is no contraction in substrate plan. GISAXS interreticular distances measured in q_z are in agreement with XRD calculated distances.

The hybrid layer, even though charged with silver salt, does not show a well-ordered mesostructure. A single XRD peak and broad GISAXS ring are obtained. XRD peak broadening and ring thickness correspond to diffraction domain coherence of about 100 nm. Layer thermal treatment leads to film contraction perpendicular to the substrate, as shown in GISAXS patterns, especially in the presence of silver salt. The observed contraction is higher in the case of F1T compared to F0T. In the first case, silver nanoparticles are formed in places initially occupied by block copolymer micelles.[22] The shrinkage is higher in F1T than in F0T. In the first case, silver nanoparticles have been formed in locations which were occupied by block copolymer micelles,[22] while empty pores are present in F0T. The silver nanoparticle formation mechanism during thermal treatment involves silver atom coalescence coming from the Ag^+ reduction present inside the silica walls.[22] This phenomenon involves the silica walls contraction around silver nanoparticles. In the other case (F0T), pore creation involves only the block copolymer elimination with gaseous species departure. In this case, silica walls do not contract themselves. Rings become more intensive after thermal treatment as block copolymer has been eliminated.

Study of GISAXS Patterns Slices in the F1T Sample. Using IGOR software,[38] a one-dimensional cross-sectional scan along the q_y direction at $q_z = 1.2\ \text{nm}^{-1}$ has been plotted. Analysis of

dx.doi.org/10.1021/jp207207x |J. Phys. Chem. C XXXX, XXX, 000–000

horizontal slices, for low q values (for $q \times R_g < 1$), according to the Guinier law,[39−42] allows us to calculate a gyration radius R_g of diffusing objects, when there is no spatial correlation between these objects. Guinier's law application conditions are met in the case of the F1T sample (Figure 3a). From the slope of the line ($\log I = f(q^2)$) (Figure 3b), the silver nanoparticle gyration radius is equal to 5.3 ± 0.5 nm, using the formula $R_g = (-3 \times \text{slope}/\ln e)^{1/2}$.

3.2. Effect of $NaBH_4$ Reduction on the Textural Properties of Hybrid Block Copolymer Silica Film. XRD patterns of the F0N sample (Figure 4a) look like the F0 pattern. It shows that the sodium borohydride treatment does not modify the layer. On the other hand, XRD patterns of the F1N sample are strongly modified since four broad peaks are observed. The two first peaks are much more intensive.

Peaks at 8.7 nm (2θ = 1.00°), 5.0 nm (2θ = 1.58°), and 4.2−4.0 nm (2θ = 2.13°) are, respectively, due to {110}, {211}, and {220}−{310} plans in Im-3m structure. It seems "a priori" quite difficult to interpret the peak at 7.8 nm (1.13°). The high intensity of the first peak leads us to conclude that the layer is predominantly orientated perpendicularly to the $\langle 011 \rangle_{cubic}$ direction.

The top-view TEM image of sample F1N, in Figure 4b, allows observation of lines spaced from 12 nm. Lines are parallel inside zones of a few hundreds of nanometers long. This view is coherent with layer reticular plans stacking perpendicularly to one direction, $\langle 011 \rangle_{cubic}$. Lines mark {0−11} trace plans. Thereby, the layer keeps the same orientation along parallel directions to substrate in different zones overlapping according to allowed twins in Im-3m structure.

The substrate perpendicular section in Figure 4c completes data in Figure 4a and 4b confirming precedent interpretations. Thereby, in this pattern, parallel layers to the substrate, micelles containing, are spaced from 9.0 nm according to interreticular distance measured with the first XRD peak in Figure 4a. The $Im\bar{3}m$ deriving structure is occurring, orientated in such a way that the $\langle 011 \rangle_{cubic}$ direction is perpendicular to the substrate. Yet, this structure observed along [11−1] azimuth in Figure 4c is contracted along $\langle 011 \rangle_{cubic}$ and becomes *Fmmm*. This picture reveals silver nanoparticle repartition inside superficial layers according to previous studies, using RBS.[22] It appears that distances between the first layers are only 8.1 nm. It allows us to explain the existence of the broad diffraction peak in Figure 4a, corresponding to a 7.8 nm distance, which has not been yet attributed.

The GISAXS pattern of the F1N sample in Figure 5a is much different from previous patterns. It is constituted with spots more or less elongated along q_z. GISAXS simulations obtained for the Im-3m structure with different orientations [011], [111] from refs 43−45 and also with [211] orientation perpendicular to the

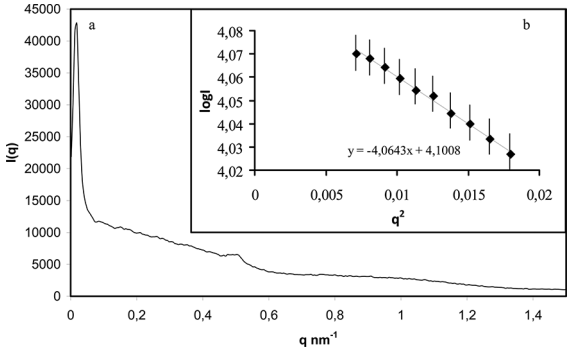

Figure 3. (a) Horizontal slice at q_z = 1.2 nm^{-1} of the F1T GISAXS pattern (Figure 2d). (b) Guinier's straight line.

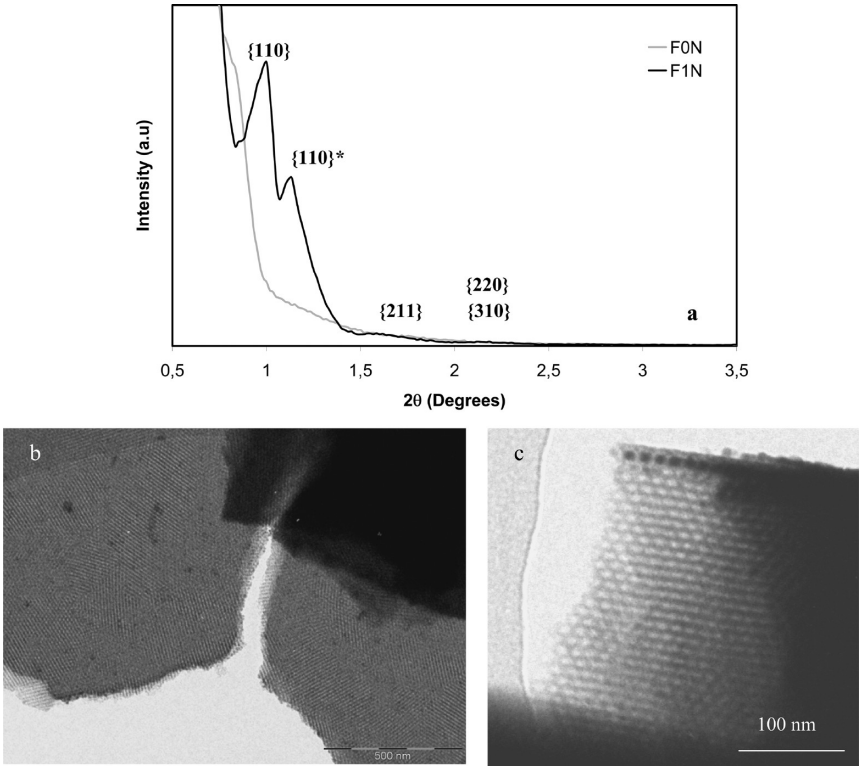

Figure 4. (a) Small-angle XRD pattern of the F1N sample; * probably corresponding to the superficial layers. (b) TEM top view of the F1N sample. (c) TEM cross-section of the F1N sample. Zone axis [11−1].

dx.doi.org/10.1021/jp207207x | J. Phys. Chem. C XXXX, XXX, 000–000

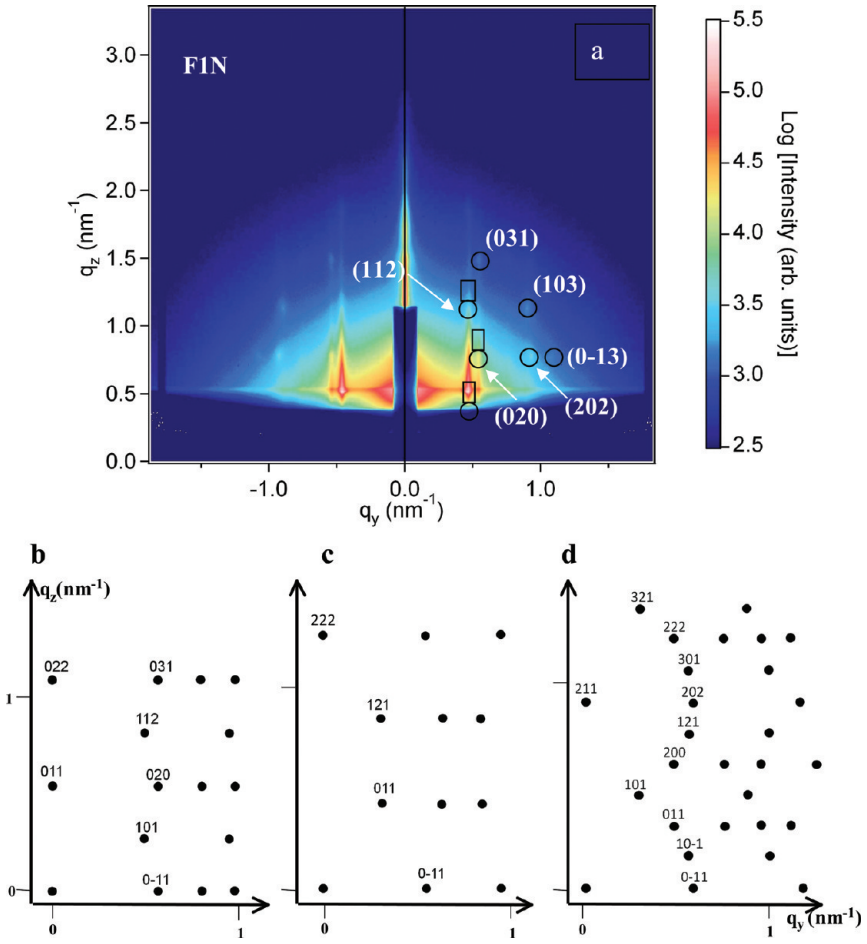

Figure 5. (a) GISAXS pattern of the F1N sample (cubic indexation). (b−d) GISAXS pattern schemes for the Im-3m structure according to orientations with different directions perpendicular to the substrate: (b) [011] direction;[43] (c) [111] direction;[43] (d) [211] direction. Patterns have been simulated with a cubic unit cell at 16 nm.

substrate are shown in Figures 5b, 5c, and 5d. Comparison with experimental data allows us to consider the preferential orientation along [011]. Yet, layer contraction, perpendicularly to the substrate, in the [011] direction changes spot position. Interreticular distances and ϕ angles calculated and measured values are compared in Table 2. The angle ϕ designs an angle between the segment formed with a given spot and origin and vertical direction ((011) spot direction). Calculated values have been obtained using the following parameters in the orthorhombic unit cell: a = 16.4 nm, b = 17.3 nm, and c = 23.1 nm. These parameter values are deduced from XRD patterns and TEM observations. Diffraction spots of Figure 5a are indexed according to Im-3m structure (and according to *Fmmm* structure in Supporting Information). The corresponding indexation in the *Fmmm* space group is reported in the Table 2. Circles correspond to direct beam spots, and squares correspond to reflected beam.

After $NaBH_4$ treatment and silver nanoparticle formation, the mesostructure is better organized, as shown in the appearance of multiple diffraction peaks in the XRD pattern and spots in the GISAXS one. Spots are explained with orthorhombic unit cell existence. Furthermore, the preferential orientation layer is noted, with the $(020)_{orthorhombic}$ plan parallel to the substrate. The elliptic form spot, with high axis parallel to q_z, is three times higher than the small axis. The monocrystalline area expands in depth of layer on 150 nm and in parallel to layer directions on 400−500 nm. This structure and this orientation are fully in agreement with TEM observations performed on thin sections taken off parallel to the direction perpendicular to the layer (Figure 4). Furthermore, they allow us to explain the appearance of the top-view layer TEM image (Figure 6a). In this case, silver nanoparticles are most often organized along "hexagons" which should not be confused with regular hexagons resulting from a cubic mesostructure with layer orientated parallel to the (111) plan. Thereby, we should attribute these geometrical figures formations to silver nanoparticles growing inside micelle positions showing on the surface (Figure 6b and 6c), with [011] orientated perpendicularly to the substrate. These nanoparticles are organized orderly according to the *cmm* space group. The parameters c/a ratio for the *cmm* unit cell deriving from nondeformed Im-3m structure is calculated as $\sqrt{2}$ (Figures 6b and 6c), as this ratio is $\sqrt{3}$ for a perfect hexagonal lattice described with a base-centered orthorhombic unit cell. Experimentally, we measure with image and FFT in Figure 6a a value equal to 1.4. From Figure 6d, this ratio is found slightly higher than 1.4; it is determined between particles localized in the same plan, as shown from neatness of the high-magnification TEM image (Figure 6d). A value of 1.41 is calculated with orthorhombic unit cell parameters deduced from XRD and TEM and according to GISAXS.

GISAXS experiments allow us to confirm that TEM observations correspond to structuration and orientation involving all

dx.doi.org/10.1021/jp207207x |*J. Phys. Chem. C* XXXX, XXX, 000–000

Table 2. Interreticular Distances and ϕ Angles: Calculated and Measured Values in Figure 5

$(hkl)_{orthorhombic}$	$(hkl)_{cubic}$	$d_{measured}$ (nm)	$d_{calculated}$ (nm)	$\varphi_{measured}$ (°)	$\varphi_{calculated}$ (°)
131	112	5.2	5.30	23	23.3
222	202	5.2	5.29	51	52.3
024	0−13	4.7	4.80	55	56.3
133	103	4.4	4.44	39	39.6
04−2	031	4.0	4.05	21	20.5

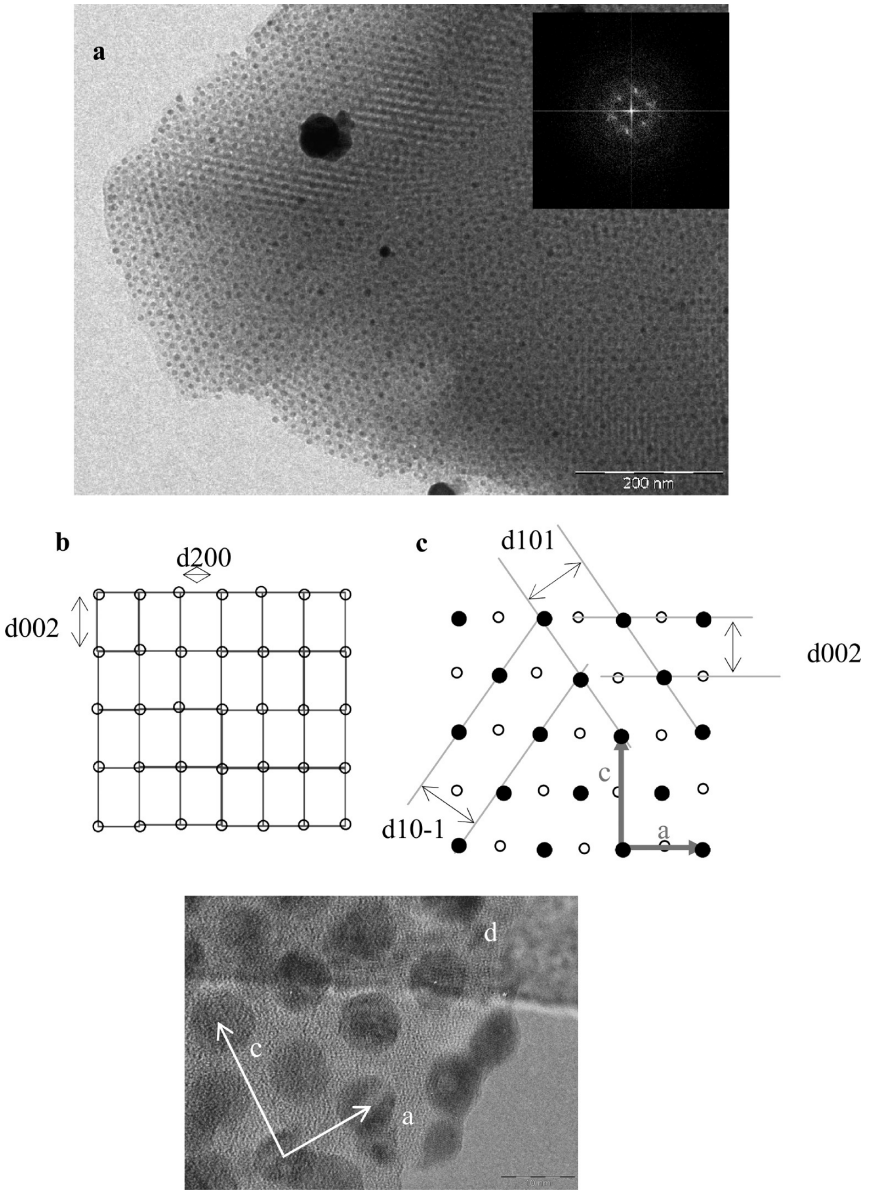

Figure 6. (a) TEM top view of the F1N sample. (b) Scheme of the top view before reduction; the layer is orientated with (011) parallel to the substrate. Empty circles figure micelle position which are not all in the sheet plan. (c) Scheme of the TEM view of the layer with (011) plans parallel to substrate, after reduction. Full circles are silver nanoparticle positions which are all in the sheet plan. Empty circles are micelle positions which are all in the same underlying plan. Ag^+ ions, coming from the depth, have all passed through these last positions. (d) Higher-magnification TEM view.

the layers after formation of silver nanoparticles. This orientation results from diffusion according to preferential ways[34] in a draft of *Fmmm* structure preexisting in the nonreduced layer. Oriented diffusion of Ag^+ ions occurs along directions ⟨111⟩ since ellipsoids of copolymer stretched along this direction, linking F127 micelles.[34,46] Ensuing this diffusion movement, the initially tenuous orientation with the direction [011] perpendicular to the substrate, becomes dominant inside all the layer thickness. In this orientation, there are eight possible diffusion ways for the unit cell to split in two sets; the first set corresponds to the four

dx.doi.org/10.1021/jp207207x |*J. Phys. Chem. C* XXXX, XXX, 000–000

shorter ways, in a plan perpendicular to the substrate; the other set consists in the four other longer ways, in a plan parallel to the substrate. Naturally, Ag^+ ions attracted by chemical reaction follow ways leading more rapidly to the layer surface. Then, the last nanoparticle monolayer looks like the top-view that is shown in Figure 6a, silver ions choosing the shorter diffusion way. This description of layer reorganization occurring during reduction involves a crystalline structure reconstruction mechanism. This is possible since the layer may not be very rigid, and most of the film is initially orientated near ⟨011⟩. Thereby, for instance, 30° oscillation around the ⟨100⟩ edge on which the unit cell lies is enough to obtain the ring pattern in Figure 1. In the Im-3m structure, plans (with high density) {100}, {111}, and {110} have micelle densities, respectively, in the ratio 1, $1/\sqrt{3}$, $\sqrt{2}$. The highest density of {110} plans explains layer preferential orientation along these plans parallel to the substrate.

The existence of two interreticular distances for parallel plans to the substrate is experimentally evidenced by two peaks "011" in the XRD pattern, by the apparition of stretched spots along q_z in the GISAXS pattern, and by TEM observations. It proves that silver diffusion occurs under the ionic form (Ag^+) from deep layers, leading to $d(011)$ around 9 nm for these layers. It also proves that the chemical reaction, Ag^+ reduction with $NaBH_4$, only concerns the superficial layers. Shrinkage along the perpendicular direction to the substrate, as in the case of F1T, is higher, and $d(011)$ becomes lower than 8 nm.

4. CONCLUSION

Results have demonstrated the important and very specific influence of $NaBH_4$ reduction in these silver salt charged films. Physico-chemical phenomena localized and directed, induced by this reduction, lead to an improvement of mesostructure and to preferential orientation well characterized by GISAXS patterns. Films after reduction have the contracted Im-3m mesostructure and are oriented with the [011] direction perpendicular to the substrate.

As thermal treatments induce nondirected phenomena and do not have such influence on film texture, they induce the film contraction, but the mesostructure remains similar to the initial one, without preferential orientation. The film contraction is much more strong when silver salt is present. We note good agreement between data from GISAXS patterns and data from XRD and TEM analyses. Slices analysis of some of the GISAXS patterns allow us to specify the diffusing objects size.

■ ASSOCIATED CONTENT

Ⓢ Supporting Information. GISAXS pattern of F1T sample (diffraction spots indexed in *Fmmm*). This material is available free of charge via the Internet at http://pubs.acs.org.

■ AUTHOR INFORMATION

Corresponding Author

*E-mail: fernand.chassagneux.@univ-lyon1.fr. Phone: 33 04 72 44 81 66. Fax: 33 04 72 44 06 18.

■ ACKNOWLEDGMENT

This work is supported by the ANR POMESCO project. We thank N. Boudet, J.F. Bérar, B. Caillot and all the d2am team.

■ REFERENCES

(1) Kreibig, U.; Vollmer, M. *Optical Properties of Metal Clusters*; Springer: Berlin, 1995.
(2) Haes, A. J.; Van Duyne, R. P. *J. Am. Chem. Soc.* **2002**, *124*, 10596.
(3) Raschke, G.; Kowarik, S.; Franzl, T.; Sönnichsen, C.; Klar, T. A.; Nichtl, J. A.; Ku1rzinger, K. *Nano Lett.* **2003**, *3*, 935.
(4) Murphy, C. J.; Gole, A. M.; Hunyadi, S. E.; Stone, J. W.; Sisco, P. N.; Alkilany, A.; Kinard, B. E.; Hankins, P. *Chem. Commun.* **2008**, 544.
(5) Pérez-Juste, J.; Pastoriza-Santos, I.; Liz-Marzan, L. M.; Mulvaney, P. *Coord. Chem. Rev.* **2005**, *249*, 1870.
(6) Bronstein, L. M. *Top. Curr. Chem.* **2003**, *226*, 55.
(7) Gacoin, T.; Besson, S.; Boilot, J. P. *J. Phys. Condens. Matter* **2006**, *18*, S85.
(8) Besson, S.; Gacoin, T.; Ricolleau, C.; Boilot, J.-P. *Chem. Commun.* **2003**, *9*, 360.
(9) Eustis, S.; Krylova, G.; Smirnova, N.; Eremenko, A.; Tabor, C.; Huang, W.; El-Sayed, M. A. *J. Photochem. Photobiol. A: Chem.* **2006**, *181*, 385.
(10) Fuertes, M. C.; Marchena, M.; Marchi, M. C.; Wolosiuk, A.; Soler-Illia, G. J. A. A. *Small* **2009**, *5*, 272.
(11) Dag, O.; Samarskaya, O.; Coombs, N.; Ozin, G. A. *J. Mater. Chem.* **2003**, *13*, 328.
(12) Valverde-Aguilar, G.; Renteria, V.; Garcia-Macedo, J. A. *Proc. SPIE* **2007**, 6641.
(13) Sun, Y.; Xia, Y. *Analyst* **2003**, *128*, 686.
(14) Chatterjee, U.; Jewrajka, S. K. *J. Colloid Interface Sci.* **2007**, *313*, 717.
(15) Solomon, S. D.; Bahadory, M.; Jeyarajasingam, A. V.; Rutkowsky, S. A.; Boritz, C. *J. Chem. Educ.* **2007**, *84*, 322.
(16) Fang, Y. *J. Chem. Phys.* **1998**, *108*, 4315.
(17) Adhyapak, P. V.; Karandikar, P.; Vijayamohanan, K.; Athawale, A. A.; Chandwadkar, A. J. *Mater. Lett.* **2004**, *58*, 1168.
(18) Park, J. H.; Park, J. K.; Shin, H. Y. *Mater. Lett.* **2007**, *61*, 156.
(19) Bois, L.; Bessueille, F.; Chassagneux, F.; Battie, Y.; Destouches, N.; Hubert, C.; Boukenter, A.; Parola, S. *Colloids Surf. A* **2008**, *325*, 86.
(20) Bois, L.; Chassagneux, F.; Battie, Y.; Bessueille, F.; Mollet, L.; Parola, S.; Destouches, N.; Toulhoat, N.; Moncoffre., N. *Langmuir* **2010**, *26* (2), 1199.
(21) Battie, Y.; Destouches, N.; Bois, L.; Chassagneux, F.; Moncoffre, N.; Toulhoat, N.; Jamon, D.; Ouerdane, Y.; Parola, S.; Boukenter., A. *J. Nanopart. Res.* **2010**, *12* (3), 1073.
(22) Bois, L.; Chassagneux, F.; Parola, S.; Bessueille, F.; Battie, Y.; Destouches, N.; Boukenter, A.; Moncoffre, N.; Toulhoat, N. *J. Solid State Chem.* **2009**, *182*, 1700.
(23) Sanchez, C.; Boissière, C.; Grosso, D.; Laberty, C.; Nicole, L. *Chem. Mater.* **2008**, *20*, 682.
(24) Nicole, L.; Boissière, C.; Grosso, D.; Sanchez, C. *J. Mater. Chem.* **2005**, *15*, 3598.
(25) Sanchez, C.; Rozes, L.; Ribot, F.; Laberty-Robert, C.; Grosso, D.; Sassoye, C.; Boissiere, C.; Nicole, L. *C. R. Chim.* **2010**, *13*, 3.
(26) Dasgupta, M.; Mahanti, M. K. *Bull. Chem. Soc. Jpn.* **1988**, *61*, 4133.
(27) Van Hyning, D. L.; Zukoski, C. F. *Langmuir* **1998**, *14*, 7034.
(28) Van Hyning, D. L.; Klemperer, W. G.; Zukoski, C. F. *Langmuir* **2001**, *17*, 3120. *Langmuir* **2001**, *17*, 3128.
(29) Jana, N. R.; Gearheart, L.; Murphy, C. J. *Chem. Commun.* **2001**, 617.
(30) Métraux, G. S.; Mirkin, C. A. *Adv. Mater.* **2005**, *4*, 412.
(31) Millstone, J. E.; Hurst, S. J.; Métraux, G. S.; Cutler, J. I.; Mirkin, C. A. *Small* **2009**, *5* (6), 646.
(32) Zhao, D.; Yang, P.; Melosh, N.; Feng, J.; Chmelka, B. F.; Stucky, G. D. *Adv. Mater.* **1998**, *10*, 1380.
(33) Soler-Illia, G. J. A. A.; Crepaldi, E. L.; Grosso, D.; Durand, D.; Sanchez, C. *Chem. Commun.* **2002**, 2298.
(34) Boissiere, C.; Grosso, D.; Lepoutre, S.; Nicole, L.; Brunet Bruneau, A.; Sanchez, C. *Langmuir* **2005**, *21*, 12362.
(35) Dourdain, S.; Bardeau, J. F.; Colas, M.; Smarsly, B.; Mehdi, A.; Ocko, B. M.; Gibaud, A. *Appl. Phys. Lett.* **2005**, *86*, 11.

(36) Besson, S.; Ricolleau, C.; Gacoin, T.; Jacquiod, C.; Boilot, J. P. *Microporous Mesoporous Mater.* **2003**, *60*, 43.
(37) Gibaud, A.; Dourdain, S.; Vignaud, G. *Appl. Surf. Sci.* **2006**, *253*, 3.
(38) *Igor Software*; WaveMetrics, Inc.: USA.
(39) Renaud, G.; Lazzari, R.; Leroy, F. *Surf. Sci. Rep.* **2009**, *64*, 255.
(40) Guinier, A. *Théorie et Techniques de la Radiocristallographie*; Dunod: France, 1956.
(41) Chojnowski, G.; Przeniosło, R.; Sosnowska, I.; Bukowski, M.; Natter, H.; Hempelmann, R.; Fitch, A.; Urban, V. *J. Phys. Chem. C* **2007**, *111*, 5599.
(42) Winans, R. E.; Vajda, S.; Lee, B.; Riley, S. J.; Seifert, S.; Tikhonov, G Y.; Tomczyk, N. A. *J. Phys. Chem. B* **2004**, *108*, 18105.
(43) Tate, M. P.; Hillhouse, H. W. *J. Phys. Chem. C* **2007**, *111*, 7645.
(44) Tate, M. P.; Urade, V. N.; Kowalski, J. D.; Wei, T. C.; Hamilton, B. D.; Eggiman, B. W.; Hillhouse, H. W. *J. Phys. Chem. B* **2006**, *110* (20), 9882.
(45) Tanaka, S.; Katayama, Y.; Tate, M. P.; Hillhouse, H. W.; Miyake, Y. *J. Mater. Chem.* **2007**, *17*, 3639.
(46) Fan, J.; Yu, C.; Gao, F.; Lei, J.; Tian, B.; Wang, L.; Luo, Q.; Tu, B.; Zhou, W.; Zhao, D. *Angew. Chem., Int. Ed.* **2003**, *42*, 3146.